Photodegradation of Rhodamine-B using Gallium Hybrids as an Efficient Photocatalyst

Kousar Parveen (kosar_ahmed111@yahoo.com)
Fatima jinnah women university, rawalpindi
Uzaira Rafique
Fatima Jinnah Women University

Research Article

Keywords: Gallium Oxide, Indole, hybrids, Photodegradation, Pseudo-first order, Rhodamine B

Posted Date: January 24th, 2022

DOI: https://doi.org/10.21203/rs.3.rs-1100461/v1

Abstract

Rhodamine B is a cationic xanthene dye widely used in the printing, textile, photography, and pharmaceutical industries. It is also well-recognized as water fluorescent and dyes laser material because of its good stability. It is toxic to human beings irritating the skin, and eyes. The present study is designed to study the photodegradation of Rhodamine B using gallium oxide and gallium hybrids as photocatalyst. Precipitation coupled with the sonochemical method is adopted for the synthesis of gallium oxide while the post grafting method is adopted for the synthesis of gallium hybrids with the indole and its derivatives. FTIR spectra showed the characteristic absorption bands of gallium oxide and gallium hybrids at 400-700 cm^{-1} and 1400-1600 cm^{-1}. SEM and XRD showed the micro-sized rectangular rod-shaped gallium oxide with rhombohedral geometry. The BET isotherm revealed the adsorption type-IV and hysteresis loop (H3) proposing multilayer and mesoporous structures. XPS confirmed the presence of gallium, oxygen, nitrogen, and carbon. The gallium oxide and gallium hybrids showed 47-72% optimum degradation of Rhodamine B under two hours of illumination at pH 7 and 0.03mg/L. The degradation rate followed a Langmuir-Hinshelwood model with R^2 >0.9.

1. Introduction

Dyes are ionizing and aromatic organic compounds showed an affinity towards the substrate to which it is being applied. It contained compounds, such as benzene, xanthene, and aromatic amines, potentially hazardous to living organisms. It entered into water bodies from the effluent of textile and dye-producing industries such as printing, paper, carpet, leather during the finishing step which has not fixed to the fibers (Kansal et al. 2009). It is estimated that more than 0.7 million tons of dyes per annum are produced worldwide (Daneshvar et al. 2012) and around 10–15% of dyes are wasted into the environment upon completion of their use in the dyeing unit (Pengthamkeerati et al. 2008). Due to its complex structure, it is marked as a non-degradable, toxic, and recalcitrant pollutant. It is responsible for causing severe allergies, and skin irritation to human. Some of them were reported as carcinogens and mutagens (Wang 2008; Ling et al. 2010). It is not only concerned with human health but also a potential threat to the quality of water and disturb the aquatic life due to eutrophication, The treatment of wastewater before releasing is a major concern of the present day. Different physicochemical techniques such as chemical coagulation, oxidation, active sludge biochemical, adsorption, chlorination, and bio-degradation have been widely used for the removal of dyes. These established techniques are often unable to reduce contaminants adequately to the desired level effectively and economically. It also produces large amounts of toxic sludge, which further needs treatment. Photo-catalysis emerged as a promising technique that helped to oxidize and mineralize the organic pollutants into carbon dioxide, water, and inorganic anions successfully. Semiconductors such as titanium oxide (Sakatani et al. 2006), zinc oxide (Yu and Yu 2008, iron oxide (Wang 2007), cadmium sulfide (Sakhthivel et al. 2003), and zinc sulfide (Sharma et al. 2012) have been reported as potential catalysts for the successful photo-degradation of different dyes Reactive blue 19, Congo red, Eriochrome black (Kansal et.al 2007; Wang et al. 2015) has been reported. Rhodamine B is a cationic xanthene dye (Sharifzade et al. 2017), widely used in the

printing, textile, photography, and pharmaceutical industries. It is also well-recognized as a water fluorescent and dyes laser material because of its good stability (Al-Kahtani 2016). Photodegradation of Rhodamine B has been reported in the literature using different photocatalyst such as titanium oxide, zinc oxide, and titanium oxide-multiwall carbon nanotubes [15, (Cotto-Maldonado et al. 2013), titanium oxide and zinc oxide/β-Cyclodextrin (Rajalakshmi et al. 2017), Zinc-graphene-titanium (Nuengmatcha et al. 2016), and many others.

Gallium oxide offers several advantages being transparent, stable with remarkable thermal and electrical properties. It also exists in α, β, γ, δ, ε polymorphic forms (Stepanov et al.2016). Different methods such as sol-gel (Tsay et al. 2012), direct precipitation (Shan et al. 2017), wet chemical (Qian et al. 2008), forced hydrolysis (Kang et al. 2015), thermal evaporation (Zhang et al. 2013), hydrothermal (Reddy et al. 2015), microwave-assisted (Deshmane et al. 2010), and electrochemical (Norizzawati et al. 2014) have been reported for the synthesis of gallium oxide. While sonochemical method (Kumar et al. 2015) is reported as a facile, efficient, and environmentally benign route, where ultrasound waves interacted with liquid media and produce acoustic cavitation. Acoustic cavitation is the formation, growth, and collapse of microbubbles. When microbubbles collapsed generates physical (shock waves, microjets, turbulence, and shear forces) and chemical (active radical) effects. These physical and chemical changes can be utilized for different applications such as cleaning, emulsification, extraction, synthesis of metal oxide, nanomaterials, hybrids, polymers. Wongpisutpaisan et al. (2011) synthesized the copper oxide nanoparticle using sonication. Guo et al. (2011), synthesized titanium/graphene oxide under sonication (20 kHz) for one hour and used it as a photocatalyst for the photodegradation of methylene blue. Similarly, Reheman et al. (2018) synthesized graphene/silver oxide quantum dot under sonication (20 kHz), and use it as a photocatalyst for the photodegradation of methylene blue. As Literature reported the remarkable application of the sonochemical method for the synthetic useful material. Therefore, the present research is designed to synthesize the gallium oxide and gallium hybrids using precipitation coupled with the sonochemical method and post-grafting method gallium hybrids. To the best of my knowledge, the present research is the first attempt to synthesize gallium hybrid with indole group under sonication and tested as photocatalyst for photodegradation of Rhodamine B. Indole is the heterocyclic compound having excessive π-electron and have great potential for oxidative coupling with different metals such as cobalt (Liu et al. 2016), and gold (Joshi et al. 2012)) via an electrophilic and nucleophilic substitution. It is also less toxic, and present in the structure of the natural product such as auxin, an amino acid.

2. Experimental Details

2.1. Materials

Gallium nitrate hydrate (99.9 %), 3-aminopropyltiethoxysilane (99 %), indole (>99 %), carboxylic acid-2-indole (98 %), 2-methyl indole (98 %), Rhodamine B (>99.9 %) were purchased from Sigma-Aldrich Co. LLC (Australia). Ammonium solution (28 %), Acetonitrile (>99.9 %), dichloromethane (>99.9 %), were purchased from Merck. All the chemical reagents were of analytical grade.

2.2. Methods

2.2.1. Synthesis of Gallium oxide

Gallium oxide and was synthesized using precipitation coupled with the sonochemical method as reported in our previous research article (Parveen et al. 2018). Briefly, 2.5 g of gallium nitrate hydrate was dissolved in 100 mL of MilliQ water, and pH is adjusted at 8 using 10 % ammonia solution. The solution was ultra-sonicated for 1 h at room temperature under Branson Digital Sonifier (S-250D, 20 kHz, and 40 W/cm^2). Then the obtained precipitates of gallium oxide were purified through washing, centrifuged (6500 rpm, 20 min), and calcined (500 $^{\circ}C$, @10 $^{\circ}C$/minute for 4 h). The synthesized gallium oxide was coded as G.

For surface activation, gallium oxide was charged with APTES as a bridging agent (Fernández et al. 2015; Yu et al. 2013; Iqbal et al. 2014; Devaraju et al. 2013) to enhance compatibility towards incoming indole groups. For this purpose, 0.2 g of gallium oxide was stirred with 10 % APTES for six-hour, filtered, washed repeatedly with isopropanol and ethanol to remove unreactive APTES, dried, and stored for hybrid synthesis. The activated gallium oxide was coded as AG.

2.2.3. Synthesis of gallium hybrids

The post-grafting method was used for the synthesis of gallium hybrids. For this purpose, 0.15 g of activated gallium oxide (AG) was dispersed in 20 mL of dichloromethane in a reagent flask with continuous stirring. An indole solution (0.30 g in 20 mL acetonitrile) was added to it and sonicate the solution for one hour using Branson Digital Sonifier (S-250D, 20 kHz, and 40 W/cm^2). After that, the solution was left undisturbed for 60 minutes at room temperature (25 $^{\circ}C$). Thus gallium-indole hybrid was synthesized, filtered, dried in the air, and coded as GI. A similar procedure was adopted for the synthesis of other gallium hybrids with indole-2-carboxylic acid and 2-methylindole, separately, and coded as GCI and GMI. The prosed structure of gallium-indole, gallium-carboxylic indole, and gallium-methyl have shown in figure 1.

2.3. Characterization

The gallium oxide and gallium hybrids were characterized using different spectroscopic techniques such as Fourier Transform Infrared Spectrometer (Bruker IFS 113v), Scanning electron microscopy (Quanta 200 FEI), X-ray diffractometer (Bruker D8), X-ray photoelectron spectroscopy (Kratos Axis ULTRA; Thermo Scientific), Thermogravimetric analysis (Mettler Toledo AG) and Brunauer–Emmett–Teller analysis (Micrometrix Tristar 3000).

2.4. Photodegradation study of Rhodamine B

To test the potential application of gallium oxide and its hybrids as a photo-catalyst, the following bench-scale photocatalysis setup was used (see Figure 2) with a specialized photocatalysis cell (double jacket

beaker).

The photocatalysis specialized cell was equipped with a quartz window and cooling jacket. An ORIEL 100-1000 W Xenon arc lamp (wavelength =420nm; irradiance intensity = 500W/cm^2) was used as a visible light source and placed in front of the quartz window (radius=2.5cm) of the cell. To avoid the heating of the solution under illumination, cold water was circulated through the jacket, and the temperature of reaction solution was maintained at 22 $^{\circ}$C. The variables such as pH (5, 7, and 9), concentration (0.01 mg/L, 0.03 mg/L and 0.05 mg/L) of adsorbate (Rhodamine B) under illumination time (120 minutes) were studied. A fixed-dose of photocatalyst (30 mg) and fixed volume (100 ml) of rhodamine B solution was used in each photocatalysis reaction. The qualitative analysis of Rhodamine B was monitored using a UV-Vis spectrophotometer (CARY 50 Bio UV-Visible) at regular intervals (10minutes) from 400-700 nm. The characteristic absorption peak of Rhodamine B was recorded at λ_{max} 554 nm. The Photo-degradation rate was calculated using equation (1).

$$\text{Photo-degradation } (\%) = \frac{A_i - A_f}{A_f} \times 100 \quad \text{_____(1)}$$

Whereas A_i and A_f is the initial and final absorbance of the dye

2.5. Kinetic Study

The effect of different initial dye concentration on the degradation rate is explained well by kinetic model (Kumar et al. 2008). it is generally showed that the rate of reaction decreases with increase in concentration.

$$r = -dC/dt = k_{app} \times C \text{_____(2)}$$

By taking the integration of above equation having C = C_o at t=0 with C_o being the initial concentration in the bulk solution and t the reaction time, lead to expected relation.

$$\ln [C_\circ/C] = k_{app} \times C$$

Where In [C_0/C] versus time for different initial concentration of dye solution and Kapp is the apparent first order rate constant.

3. Results And Discussion

The successful application of the sonochemical method opens a new window in the field of material science for the synthesis of different novel materials. The powerful ultrasound radiation produces acoustic cavitation (formation, growth, and implosion of microbubbles) in a liquid medium. The implosion of these microbubbles generates extreme high temperature and pressure in the microscopic region (hot spots) with active radicles (hydrogen, oxygen, and hydroxyl O°, H°, OH°). These radicals are

used to initiate the chemical reaction. In the present research work, gallium oxyhydroxide is synthesized when gallium hydroxide in the presence of ammonia solution sonicated for one hour. The sonication produces active dissolved oxygen and hydroxyl radicals (Bang & Suslick 2010) that react with gallium hydroxide and synthesized the gallium oxide. Similarly, sonication is also helpful in the initiation of reaction between indole groups and activated gallium oxide.

3.1. FTIR

FTIR Spectrum of starting material (gallium oxide) showed characteristic oxygen-containing groups at 3440 cm^{-1}, 700-400 cm^{-1} assigned to stretching vibration of hydroxyl (O-H), and gallium oxide (Ga-O-Ga) present in the gallium oxide (Kang et a. 2016; Girija et al. 2015; Yang et al. 2009). The surface of gallium oxide is activated with 3-aminopropyltiethoxysilane (APTES) to make it compatible with the attachment of the incoming indole group. The IR spectrum of activated gallium oxide (see figure 3) showed distinct stretching vibrations of C-H, N-H, Si-O-Si at 2900 cm^{-1}, 3500-3300 cm^{-1}, and 1034 cm^{-1} region (Kim & Kown 2017). The broadening of the OH group occurred due to the overlapping of the amine group. Furthermore, bending absorption bands of NH, and Si-C were also noticed at 1566 cm^{-1} and 1330 cm^{-1}. The APTES is successfully attached to the surface of gallium oxide.

IR spectrum of gallium hybrids (see Figure 4) showed the distinct absorption bands of -CH (2900 cm^{-1}), -C=C (1480-1400 cm^{-1}), C-N (1340-1314 cm^{-1}), C-O (1225 cm^{-1}), C=O (2392-2341 cm^{-1}), and -NH (1600-1400 cm^{-1}). These additional absorption bands confirmed the attachment of indole with Ga-O (1132-1117 cm^{-1}) and Si-O (1030-1008 cm^{-1}) repeating units. Our study agrees with (Kumar 2015). It is also interesting to note that the benzene ring remains intact during hybrid synthesis (Joshi & Prakash 2012; Joshi et al. 2012). It means that metal bonding occurred at the active site (C_2 and C_3) of the pyrrole ring of indole (see figure 4). The coordination of different metals with indole is also investigated by other researchers (Liu et al. 2016) and (Gomez et al. 2012). However, methyl and carboxylic substituted indole group at C_2 position provided the additional attachment sites and gave more intense stretching and bending absorption bands between 1200-1500 cm^{-1}.

3.2. SEM

SEM images of gallium oxide showed the well-defined rectangular-shaped micro-rods (see Figure 5) containing void spaces. These void spaces showed the sorption site where the catalytic reaction took place.

After activation with APTES, the surface of gallium oxide showed smoothness and homogeneity. A slight distortion has been noticed in the morphology after hybrid synthesis. It is likely to observe that the indole group alter the morphology of gallium oxide and arranged the particles in the form of a chain through silane bridging. The methyl and carboxylic group substituted indole further modified particles and stacking the particles together (see Figure 6). The reorientation of micro-rods resulted in the formation of

the clumps. Hence, the effect of change in morphology is reflected in the functioning of the material. It showed that gallium hybrids adhere to the synergic property of gallium oxide and indole.

3.3. XRD

Diffraction pattern at 2θ= 24.5°(012), 33.8°(104), 36°(110), 41.4°(113), 50.2°(024), 55.1°(116), 63.4°(214), and 65°(300) proposed the trigonal system with space group $R\bar{3}c$ (167) as shown in Figure 7. This is about PDF# 43-1013. The lattice constants (a=b=4.98 Å and c=13.43 Å; α=γ=90° β= 120°) recognized α-Ga_2O_3 having no other phase as showed by Li et al. (2012). The average crystallite size of gallium oxide (26 nm) was calculated using the Debye Scherrer equation (D_{hkl}=0.9λ/β cos θ). Indole group induced no change in the basic crystal lattice of gallium oxide, however, physical attachment broadened the diffraction peaks only thus reducing crystallinity from 90 % to 32 % (Bagheri et al. 2013; Minoo Bagheri 2014; Bagheri et al. 2014), accompanied by an increase in crystallite size (from 26 nm to 32 nm) as shown in Figure 7. It is likely to mention that percentage of amorphous is calculated using XRD software.

3.4. BET

Adsorption-desorption of nitrogen onto gallium oxide followed adsorption type-IV (see supplementary information, S1). BET isotherm proposing multilayer adsorption forming a hysteresis loop (H3) which is the signature of mesoporous particles of gallium oxide according to the IUPAC classification 1985 (Sing 1985). The maximum specific surface area, pore-volume, and pore diameter calculated are 26 m^2/g, 0.15 cm^3/g, and 34 nm, respectively. While the BET isotherm of gallium hybrids showed similar characteristics as noted earlier for gallium oxide, i.e., hysteresis loop (H3), adsorption type-IV (Zhao et al. 2007) as shown in figure 8 b, c, d. However, an increase in surface area is noted from 26 m^2/g (gallium oxide) to 31 m^2/g (gallium-indole), 35 m^2/g (gallium-methyl indole), and 37 m^2/g (gallium-carboxylic indole).

3.5. TGA

TGA of gallium oxide showed two-step decomposition of 2 % and 10 % mass loss, whereas holding 88 % residue depicted the thermal stability of gallium oxide (see supplementary information, S2). The results are encouraging for its application under high temperatures. While the Thermal stability of gallium hybrids was also determined. TG curve of gallium hybrids (see supplementary information, S2) showed an initial mass loss due to volatile gases and water of hydration up to 100 °C, followed by dissociation of organic from inorganic substituents up to 600 °C. In particular, each indole group revealed different weight loss, i.e., 8 %, 10 %, and 8 % for gallium-indole (GI), gallium-carboxylic indole (GCI), and gallium-methyl indole (GMI), respectively. The thermal stability sequence follows GCI > GI > GMI.

3.6. XPS

XPS survey spectrum (see supplementary file S3) of gallium oxide showed the peak of gallium (Ga $2p^{1/2}$, Ga$2p3^{/2}$), and oxygen (O 1s) peak at 1180 eV and 531 eV, confirmed the successful synthesis of Ga_2O_3

(Bharat et al. 2016). Whereas peak at 397 eV and 285 eV corresponds to N 1s and C 1s as traces (Colombo et al. 2017).The high resolution deconvoluted XPS spectrum showed gallium binding with and oxygen at ~530.4 eV and ~531.8 eV corresponding to Ga-O and Ga-OH. XPS survey spectra of gallium hybrids also displayed distinct peaks of O1s, C1s, N1s, and Ga2p at 531 eV, 285 eV, 399 eV, and 1180 eV with enhanced intensity (see supplementary file S3). The high-resolution deconvoluted XPS spectra of gallium hybrids showed distinct binding with its surrounding elements (see supplementary data, S4). The deconvoluted peak of C1s at 285 eV (C–C/C–H of benzene), 286.2-286.4 eV (C-O), 288.4-288.8 eV (C=O), and 288.2-288.6 eV (O–C=O), reflects the carbon association with oxygen such as carbon-carbon, carbonyl, and carboxylic, respectively. The deconvoluted peaks of N1s at 399.7-400.3 eV and 400-402 eV were assigned to N-C and N-H. While the deconvoluted peak of O1s at 530 eV corresponding to Ga-O, 530.5-531.2 eV (C=O), 532.1-532.6 eV (C–O–H), and 399.7-398 eV (N-O). Our findings are in good agreement with other authors (Guzman et al. 2016; Sarkar & Sampath 2016). Table 1 showed the elemental composition and percent weight of gallium oxide and gallium hybrids.

Table 1. Elemental composition of gallium oxide and gallium hybrids.

Element	G	GI	GCI	GMI
	% Atom	% Atom	% Atom	% Atom
Ga	14	3	6	10
O	31	28	29	32
C	9	46	29	18
N	46	23	36	40

3.7. Photocatalysis of Rhodamine B

The potential of gallium oxide and gallium hybrids as photocatalyst were tested in a batch mode as a function of concentration (0.01 mg/L, 0.03 mg/L, and 0.05 mg/L), pH (5 as acidic, 7 as neutral, 9 as basic), and illumination time (120 minutes) towards Rhodamine B (Rh-B).

Three preliminary experiments were also conducted for 20 minutes to clarify the role of light, and catalyst in the degradation process. (a) Dark reaction (gallium hybrids without visible light illumination), (b) Photolysis (only visible light illumination), (c) photo-catalysis reaction (gallium hybrids with visible light illumination). It has been observed that the better catalytic degradation of Rhodamine B was achieved in photo-reaction (18-36 %) over dark reaction (12-25 %) and photolysis (8-17 %) at pH 7 and 0.03 mg/L as shown in Figure 8. Thus, Photoreaction was further continued to evaluate the maximum degradation capability.

3.7.1. Gallium oxide as Photocatalyst

Gallium oxide showed 30 % photodegradation of Rh-B at 0.03 mg/L while 47 % at pH 7 as shown in figure 9. It was found that photodegradation of rhodamine B was gradually increased with an increase in

illumination time. When more light falls on the catalyst surface, it enhanced the formation of more photo excited species, increased the photodegradation. The decrease in the photodegradation rate at high concentrations (0.05 mg/L) is due to less penetration of photons into the dye solution. The same trend was also observed in another study (Al-Kahtani 2016). pH is another important variable that affects the photodegradation process. It changed the surface chemistry of photocatalyst and dye molecule that shifts the photodegradation rate. The surface of gallium oxide and Rhodamine B at pH 5 gets protonated and acts as Lewis acid. So, less photodegradation (37 %) is achieved due to the electrostatic repulsion. The deprotonation of Rhodamine B at pH 9 resulted in the formation of a zwitter (RB^+) ion that attracted by the surface of the catalyst, the presence of hydroxyl radicle is also facilitated the dye degradation up to 40%. The same trend was also observed by Hariprasad et al. (2013). The maximum photodegradation (48 %) is achieved at pH 7 because of the unlike charge on both catalyst surface and dye molecule responsible for strong electrostatic attraction as well as less hindrance for photo-excited species to attacked and degraded the dye easily (see figure 10).

3.7.2. Gallium hybrids as Photocatalyst

Gallium hybrids showed 44-58 % photodegradation of Rhodamine B at 0.03 mg/L within 120 min. while 59-72 % photodegradation of dye is achieved at pH 7(see figure 9). The photodegradation of Rh-B is enhanced by gallium hybrid as compared to gallium oxide. It is due to the binding of the indole group onto gallium oxide. Upon exposure to light, the indole group infused more photo-generated electrons into the conduction band of gallium oxide. Our finding is further supported by Kamil et al., (2018), who studied the degradation of Bismarck brown R using hybrid (multi-wall carbon nanotubes-titanium oxide). He found that multi-wall carbon nanotubes as an electron promoter in the conduction band of titanium oxide-forming superoxide anion radicals. Rhodamine B showed optimal degradation at pH 7 due to electrostatic attraction between negatively charged catalyst surface and dye molecule. The deprotonation of Rhodamine B formed zwitter (RB^+) ion and the presence of hydroxyl radicle facilitates the degradation process (Nagaraja et al. 2012). However, in an acidic environment surface, both gallium hybrid surface of catalyst and dye molecule gets protonated and coulombic repulsion reduced the degradation process (see figure 10). Different researchers also mentioned the potential of gallium hybrid/composites for dye degradation (Banerjee et al. 2012; Kim et al. 2016; Das et al. 2019; Reddy et al. 2016).

3.7.3. Mechanism of Photocatalysis

When gallium hybrids were irradiated with visible light, the electron from the valence band of the catalysts promoted to the conduction band leaving holes in the valence band and excited electrons to the conduction band. The photoelectrons on the conduction band were scavenged by oxygen to produce reactive oxygen radicals (O°), whereas the holes in the valence band become trapped by the surface bounded hydroxyl radicals which produced on oxidation of either the surface hydroxyl group (OH) or water molecules (H_2O). These hydroxyl radicals have high oxidation potential used to oxidation of dye [14] into non-hazardous by-products (CO_2 and H_2O). The mechanisms of photodegradation are illustrated in Figure 11.

The photocatalytic activity of gallium oxide was enhanced after its binding with the indole group. Indole group helped to infuse more photo-generated electrons into the conduction band of gallium oxide upon exposure to light. Furthermore, the indole group also created defects that reduce the recombination of electrons (e^-) and holes (h^+) that pronounced the photodegradation process. The band gap of all synthesized gallium hybrids was also calculated using the Tauc plot method (see the supplementary file, S6).

3.8. Kinetic Study

This study followed the pseudo first order reaction (Kumar et al. 2007), the kinetic parameters are presented here in the tabulated form. The value of apparent rate constant is obtained from regression analysis of the linear curve of the plot.

The apparent rate constant clearly showed that the rate of degradation increases with the increase in initial concentration. While at high concentrations (0.05mg/L), the catalytic reaction becomes reduced due to less penetration of photons into the solution. The same trend was also observed in another study (Al-Kahtani 2016).

Table 2. Kinetic Parameters of the pseudo first order.

Gallium Oxide (G)			
Induced concentration (mg/L) →	0.01	0.03	0.05
k_1(min^{-1})	2.1x10^{-3}	6.7x10^{-3}	3 x10^{-3}
R^2	0.98	0.97	0.95
Gallium indole (GI)			
k_1(min^{-1})	2.5 x10^{-2}	3.3x 10^{-2}	2.3 x10^{-2}
R^2	0.98	0.99	0.96
Gallium carboxylic indole (GCI)			
k_1(min^{-1})	4.1 x10^{-2}	5.7 x 10^{-2}	1.5 x10^{-2}
R^2	0.97	0.98	0.97
Gallium methyl indole (GMI)			
k_1(min^{-1})	3.2 x10^{-2}	4.1 x 10^{-2}	2.7 x10^{-2}
R^2	0.97	0.98	0.92

4. Conclusions

Synthesis of gallium oxide and gallium hybrids was successfully synthesized using precipitation coupled with the sonochemical method. The sonochemical method is emerged as a facile, and the time-efficient method which requires no additional chemicals during synthesis. Similarly, the post-grafting method is proved to be an efficient method for the synthesis of gallium-indole hybrids. Upon exposure to light, the indole group helped to infuse more photo-generated electrons into the conduction band of gallium oxide,

which helps the photo-degradation of Rhodamine B up to 72 % at 0.03mg/L within 20 minutes under visible light. Pseudo first order kinetic is fitted well to experimental data with R^2 >0.9.

Declarations

Ethical Approval: The authors declare that there is no financial and personal conflict of interest that could appear to influence the work reported in this paper.

Consent to Participate: All Authors declare that they equally participated in the research study and development of article.

Consent to Publish: All the authors read the final version of article and give consent to publish the article to be published in Environmental Science and pollution Research journal.

Authors Contributions: I: Kousar Parveen, the corresponding author of this manuscript certify the specific contributions made by each author. **Kousar Parveen:** Investigation, methodologies, formal analysis, writing original draft preparation, editing. **Uzaira Rafique:** Conceptualization, supervision, validation, visualization, review, and editing

Funding: This research work was supported by the Fatima Jinnah Women University, The Mall Rawalpindi.

Competing interest: The authors have no competing interests to declare that are relevant to the content of this article.

Availability of data and materials: The authors confirm that the data supporting the findings of this study are available within the article and its supplementary material. Raw data that supports the findings of this study are available from the corresponding author, upon reasonable request.

References

Al-Kahtani AA, (2016) Photocatalytic Degradation of Rhodamine B Dye in Wastewater Using Gelatin/CuS/PVA Nanocomposites under Solar Light Irradiation. J Biomater and Nanobiotechn. 8(01): 66.

Banerjee AN, Joo SW, and Min BK (2012)Photocatalytic degradation of organic dye by sol-gel-derived gallium-doped anatase titanium oxide nanoparticles for environmental remediation. J Nanomater

Bang JH and Suslick KS (2010) Applications of ultrasound to the synthesis of nanostructured materials. Adv Mater 22(10): 1039-59.

Bagheri M, Mahjoub AR, Khodadadi AA, and Mortazavi Y (2014) Fast *photocatalytic degradation of congo red using CoO-doped β-Ga2O3 nanostructures.* RSC Adv 4(63): 33262-33268.

Bharat LK, Nagaraju G, Krishna KG, and Yu JS (2016) Controlled synthesis of yttrium gallium garnet spherical nanostructures modified by silver oxide nanoparticles for enhanced photocatalytic properties. Cryst Eng Comm 18(46): 8915-8925.

Bagheri M, Khodadadi AA, Mahjoub AR, and Mortazavi Y (2013) Highly sensitive gallia-SnO_2 nanocomposite sensors to CO and ethanol in presence of methane. Sens Actuators B Chem 188: 45-52.

Colombo E, Li W, Bhangu SK, and Ashokkumar M (2017) Chitosan microspheres as a template for TiO2 and ZnO microparticles: studies on mechanism, functionalization and applications in photocatalysis and H2S removal. RSC Adv 7(31): 19373-19383.

Cotto-Maldonado M D C., Campo T, Elizalde E, Gómez-Martínez A, Morant C, & Márquez F (2013). Photocatalytic degradation of rhodamine-B under UV-visible light irradiation using different nanostructured catalysts. Chem Sci Intl J (4) 178-202.

Daneshvar E, Kousha M, Jokar M, Koutahzadeh N, and Guibal E (2012) Acidic dye biosorption onto marine brown macroalgae: isotherms, kinetic and thermodynamic studies. Chem Eng J 204: 225-234.

Das B, Das B, Das NS, Sarkar S, and Chattopadhyay KK(2019) Tailored mesoporous nanocrystalline Ga_2O_3 for dye-selective photocatalytic degradation. Micropor and Mesopor Mater 288, 109600.

Devaraju S, Vengatesan MR, Selvi M, Song JK, and Alagar M (2013) Mesoporous silica reinforced cyanate ester nanocomposites for low k dielectric applications. Micro and Meso Mater 179: 157-164.

Deshmane CA, Jasinski JB, and Carreon MA (2010) Microwave-assisted synthesis of nanocrystalline mesoporous gallium oxide. Micropor Mesopor Mat 130(1-3): 97-102.

Fernández LG et al., (2015) Synthesis and Characterization of Vinyltrimethoxysilane-Grafted Non-Swelling Clay. Procedia Mater Sci 8: 414-423.

Girija K, Thirumalairajan S, Mastelaro VR, and Mangalaraj D (2015) Photocatalytic degradation of organic pollutants by shape selective synthesis of β-Ga2O3microspheres constituted by nanospheres for environmental remediation. J. Mater. Chem. A, 3(6): 2617-2627.

Gómez Costa MB, Juárez JM, Martínez ML, Cussa J, and Anunziata OA, (2012) Synthesis and characterization of a novel composite: Polyindole included in nanostructured Al-MCM-41 material. Micropor Mesopor Mat, 153: p. 191-197.

Guo J, Zhu S, Chen Z, Li Y, Yu Z, Liu Q, Li J, Feng C, Zhang D (2011) Sonochemical synthesis of TiO2 nanoparticles on graphene for use as photocatalyst. Ultrason Sonochem 18(5): 1082-1090.

Guzmán G, Herrera M, Silva R, Vásquez GC, and Maestre D (2016) Influence of oxygen incorporation on the defect structure of GaN microrods and nanowires. An XPS and CL study. Semicond Sci Technol 31(5): 055006.

Hariprasad N, Anju S, and Yesodharan E (2013) Sunlight induced removal of Rhodamine B from water through semiconductor photocatalysis: effects of adsorption, reaction conditions and additives. Res J Mater Sci ISSN, 2320: 6055.

Iqbal MZ et al., (2014) Effect of solvent on the uncatalyzed synthesis of aminosilane-functionalized graphene. RSC Adv, 4(13): 6830-6839.

Joshi L, Singh AK, and Prakash R (2012) Polyindole/carboxylated-multiwall carbon nanotube composites produced by in-situ and interfacial polymerization. Mat Chem and Phy 135(1): 80-87.

Joshi L and Prakash R (2012) Polyindole-Au nanocomposite produced at the liquid/liquid interface. Mater Lett 66(1): 250-253.

Joshi L Singh AK, and Prakash R (2012) Polyindole/ carboxylated-multiwall carbon nanotube composites produced by in-situ and interfacial polymerization. Mater Chem Phys 135(1): 80-87.

Kamil AM, Mohammed HT, Balakit AA, Hussein FH, Bahnemann DW, and El-Hiti GA, (2018) Synthesis, Characterization and Photocatalytic Activity of Carbon Nanotube/Titanium Dioxide Nanocomposites. Arab J Sci Eng 43(1): 199-210.

Kansal SK, Kaur N, and Singh S (2009) Photocatalytic degradation of two commercial reactive dyes in aqueous phase using nanophotocatalysts. Nanoscale Res Lett 4(7): 709.

Kansal S, Singh M, and Sud D (2007) Studies on photodegradation of two commercial dyes in aqueous phase using different photocatalysts. Journal of hazardous materials, 141(3): 581-590.

Kang BK, Lim HD, Mang SR, Song KM,. Jung MK, Kim SW, and Yoon D (2015) Synthesis and characterization of monodispersed β-Ga2O3 nanospheres via morphology controlled $Ga_4(OH).10SO_4$ precursors. Langmuir, 31(2): 833-838.

Kang BK, Lim GH, Lim B, and Yoon DH (2016)Morphology controllable synthesis and characterization of gallium compound hierarchical structures via forced-hydrolysis method. J Alloys and Compd, 675: 57-63.

Kumar KV, Porkodi K, and Rocha F (2008) Langmuir–Hinshelwood kinetics – A theoretical study. Catal. Commun. 9(1): 82-84.

Kim S, Han KI, Lee IG, Park WK, Yoon Y, Yoo CS, Yang WS, and Hwang WS (2016) A gallium oxide-graphene oxide hybrid composite for enhanced photocatalytic reaction. Nanomaterials, 6(7), 127.

Kim H and Kwon JY, (2017) Enzyme immobilization on metal oxide semiconductors exploiting amine functionalized layer. RSC Adv 7(32): 19656-19661.

Kumar T M (2015) Biofield Treatment: A Potential Strategy for Modification of Physical and Thermal Properties of Indole. J Environ Anal Chem 02(04).

Kumar VB, Gedanken A, and Porat ZE (2015) Facile synthesis of gallium oxide hydroxide by ultrasonic irradiation of molten gallium in water. Ultrason Sonochem, 26: 340-344.

Kumar KV, Porkodi K, and Selvaganapathi A (2007) Constrain in solving Langmuir–Hinshelwood kinetic expression for the photocatalytic degradation of Auramine O aqueous solutions by ZnO catalyst. Dyes and Pigm 75(1): 246-249.

Ling SK, Wang S, and Peng Y (2010) Oxidative degradation of dyes in water using Co2+/H2O2 and Co^{2+}/peroxymonosulfate. J Hazard Mater 178(1-3): 385-389.

Liu BH, Dou LT, He F, YangJ, Li ZP (2016) A cobalt coordination compound with indole acetic acid for fabrication of a high performance cathode catalyst in fuel cells. RSC Adv 6, 19025-19033.

Li L, Wei W and Behrens M (2012) Synthesis and characterization of α-, β-, and γ-Ga2O3 prepared from aqueous solutions by controlled precipitation. Solid State Sci 14(7): 971-981.

Minoo Bagheri ARM (2014) Enhanced photocatalytic degradation of congo red by solvothermally synthesized CuInSe2–ZnO nanocomposites. RSC Adv 4: 21757.

Nagaraja R, Kottam N, Girija CR, and Nagabhushana BM (2012) Photocatalytic degradation of Rhodamine B dye under UV/solar light using ZnO nanopowder synthesized by solution combustion route. Powder techn 215: 91-97.

Norizzawati MG, Kanji-Yasui MRM and Hashim AM (2014)Electrochemically deposited gallium oxide. Nanoscale Res Lett 9(120).

Nuengmatcha P, Chanthai S, Mahachai R, and Oh WC (2016) Visible light-driven photocatalytic degradation of rhodamine B and industrial dyes (texbrite BAC-L and texbrite NFW-L) by ZnO-graphene-TiO2 composite. J Env Chem Eng 4(2): 2170-2177.

Parveen K, Rafique U, Akhtar MJ, & Ashokumar M (2018) Ultrasound-assisted synthesis of gallium hybrids for environmental remediation application. Ultrason Sonochem 49, 222-232.

Pengthamkeerati P, Satapanajaru T, and Singchan O (2008) Sorption of reactive dye from aqueous solution on biomass fly ash. J Hazard Mater 153(3): p. 1149-1156.

Qian HS, Gunawan P, Zhang YX, Lin GF, Zheng JW, and Xu R (2008) Template-free synthesis of highly uniform α-GaOOH spindles and conversion to α-Ga_2O_3 and β-Ga_2O_3. Cryst. Growth Des.8(4): 1282-1287.

Rajalakshmi S, Pitchaimuthu S, Kannan N, and Velusamy P (2017) Enhanced photocatalytic activity of metal oxides/β-cyclodextrin nanocomposites for decoloration of Rhodamine B dye under solar light irradiation. Appl Water Sci **7**(1): p. 115-127.

Reddy LS, Ko YH, and Yu JS, (2015). Hydrothermal synthesis and photocatalytic property of β-Ga_2O_3 nanorods. Nanoscale Res Lett 10(1): 364.

Reheman A, Tursun Y, Dilinuer T, Halidan M, Kadeer K, and Abulizi A (2018) Facile One-Step Sonochemical Synthesis and Photocatalytic Properties of Graphene/Ag_3PO_4 Quantum Dots Composites. Nanoscale Res Lett 13(1): 70.

Reddy LS, Ko YH, and Yu JS (2015)Hydrothermal synthesis and photocatalytic property of β-Ga_2O_3 nanorods. Nanoscale Res Lett 10(1), 1-7.

Sakatani Y, Ando H, Koike H (2006) Titanium oxide and photocatalyst. Google Patents.

Sakthivel SB, Neppolian MV, Shankar B, Arabindoo M, Palanichamy, Murugesan VM (2003) Solar photocatalytic degradation of azo dye: comparison of photocatalytic efficiency of ZnO and TiO_2. Sol. Energy Mater Sol. Cells 77(1): p. 65-82.

Sarkar S and Sampath S (2016) Ambient temperature deposition of gallium nitride/gallium oxynitride from a deep eutectic electrolyte, under potential control. ChemComm, 52(38): 6407-6410.

Sharma M, Jain T, Singh S, and Pandey O P (2012) Photocatalytic degradation of organic dyes under UV–Visible light using capped ZnS nanoparticles. Sol Energy 86(1): 626-633.

Sharifzade G, Asghari A, and Rajabi M (2017) Highly effective adsorption of xanthene dyes (rhodamine B and erythrosine B) from aqueous solutions onto lemon citrus peel active carbon: characterization, resolving analysis, optimization and mechanistic studies. RSC Adv 7(9): 5362-5371.

Sing KS (1985) Reporting physisorption data for gas/solid systems with special reference to the determination of surface area and porosity (Recommendations 1984). Pure Appl. Chem. 57(4): 603-619.

Stepanov S, Nikolaev EV, Bougrov V, and Romanov A (2016), Gallium Oxide: Properties And Applica A Review. Rev. Adv. Mater. Sci, 44: 63-86.

Shan JJ, Li CH, Wu JM, Liu JA, and Shi YS (2017) Shape-controlled synthesis of monodispersed beta-gallium oxide crystals by a simple precipitation technique. Ceram Intl 43(8): 6430-6436.

Tsay CY, Fan KS, and Lei CM (2012) Synthesis and characterization of sol–gel derived gallium-doped zinc oxide thin films. J. Alloys Compd 512(1): 216-222.

Wang CT (2007), Photocatalytic activity of nanoparticle gold/iron oxide aerogels for azo dye degradation. J Non Cryst Solids 353(11-12):1126-1133.

Wang S (2008) A comparative study of Fenton and Fenton-like reaction kinetics in decolourisation of wastewater. Dyes Pigm 76(3): 714-720.

Wang F, Li FL, Xu MM, Yu H, Zhang JG, Xia HT, and Lang JP(2015) Facile synthesis of a Ag (i)-doped coordination polymer with enhanced catalytic performance in the photodegradation of azo dyes in water. J Mater Chem A 3(11): p. 5908-5916.

Wongpisutpaisan N, Charoonsuk P, Vittayakorn N, & Pecharapa W (2011) Sonochemical synthesis and characterization of copper oxide nanoparticles. Energy Procedia 9:404-409.

Yang JJ, Zhao Y, and Frost RL (2009) Infrared and infrared emission spectroscopy of gallium oxide alpha-GaO(OH) nanostructures. Spectrochim Acta A Mol Biomol Spectrosc 74(2): 398-403.

Yu B et al., (2013) Enhanced thermal and mechanical properties of functionalized graphene/thiol-ene systems by photopolymerization technology. Chem Eng J, 228: 318-326.

Yu J and Yu X, Hydrothermal synthesis and photocatalytic activity of zinc oxide hollow spheres. Environ. Sci. Technol 42(13): 4902-4907.

Zhang, T, Lin J, Zhang X, Huang Y, Xu X, Xue Y, Zou J, and Tang C (2013) Single-crystalline spherical β-Ga 2 O 3 particles: synthesis, N-doping and photoluminescence properties. J Lumin, 140: 30-37.

Zhao Y, Frost RL, and Martens WN(2007) Synthesis and characterization of gallium oxide nanostructures via a soft-chemistry route. J Phys Chem C, 111(44): 16290-16299.

Figures

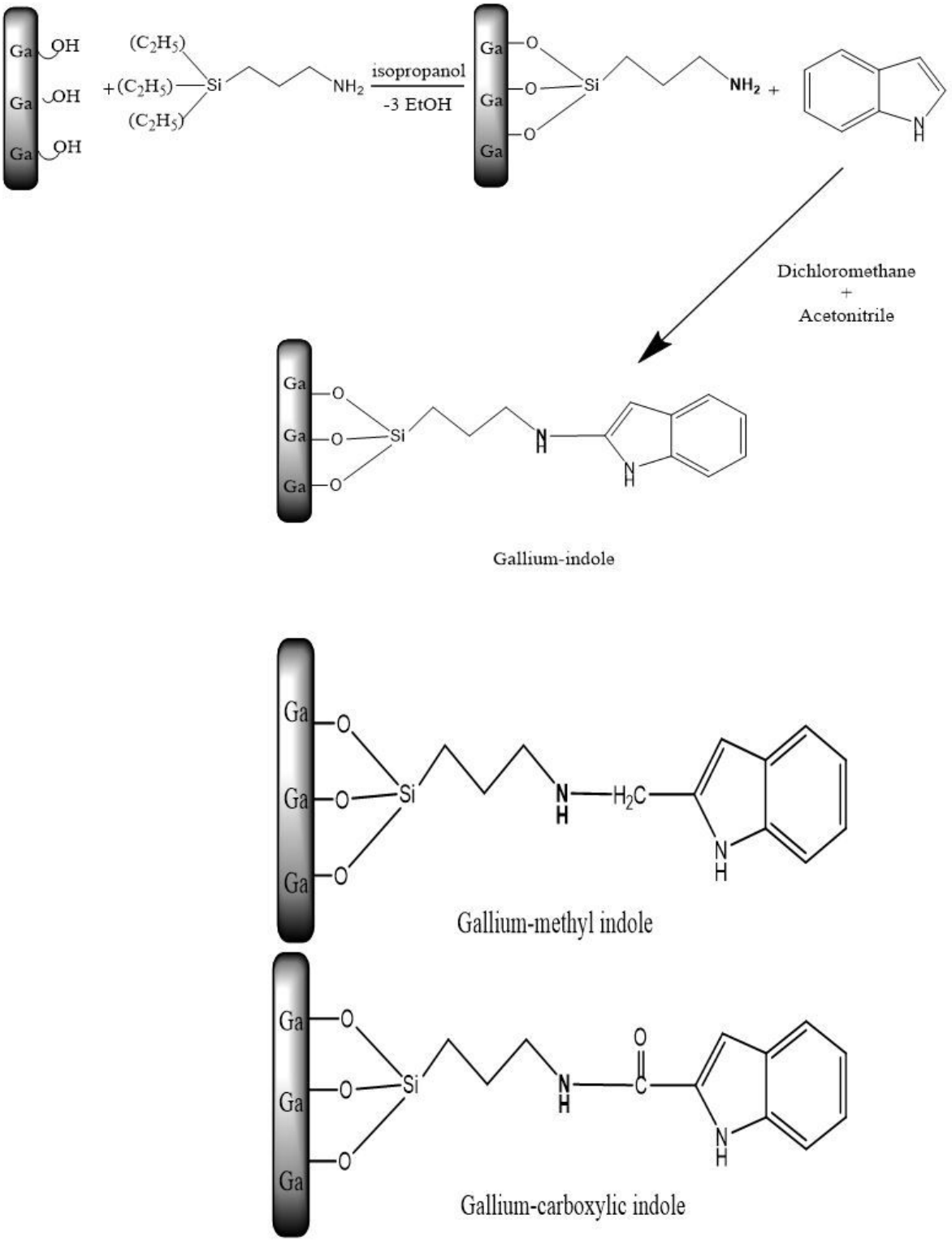

Figure 1

Proposed structure of gallium oxide and gallium hybrids.

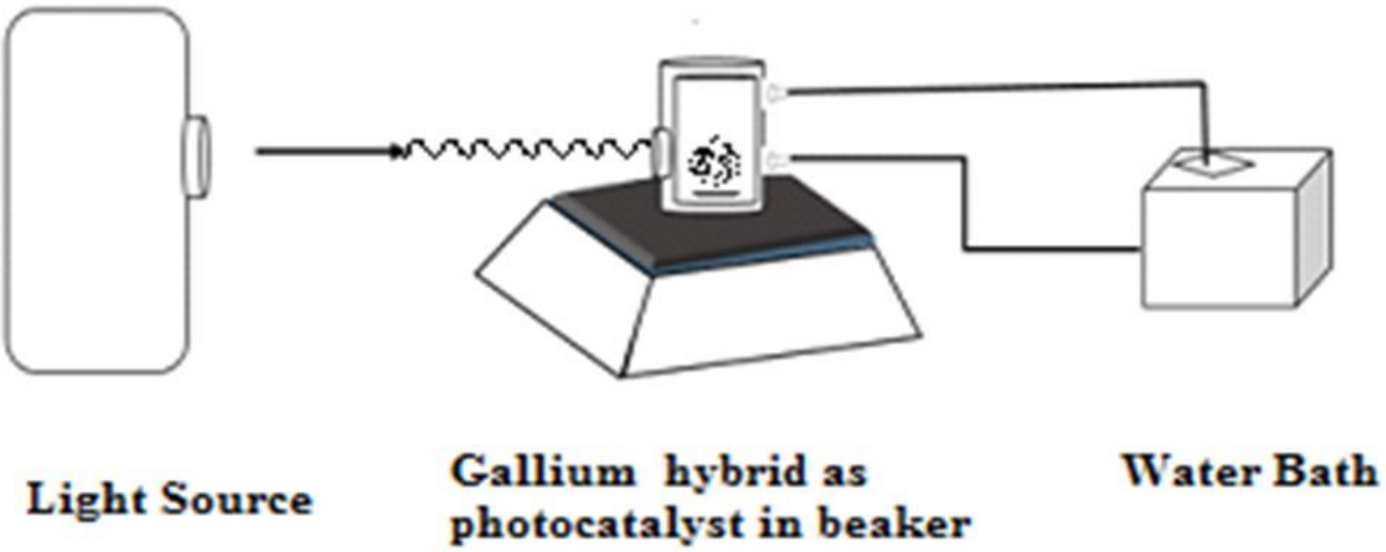

Figure 2

Photocatalysis setup.

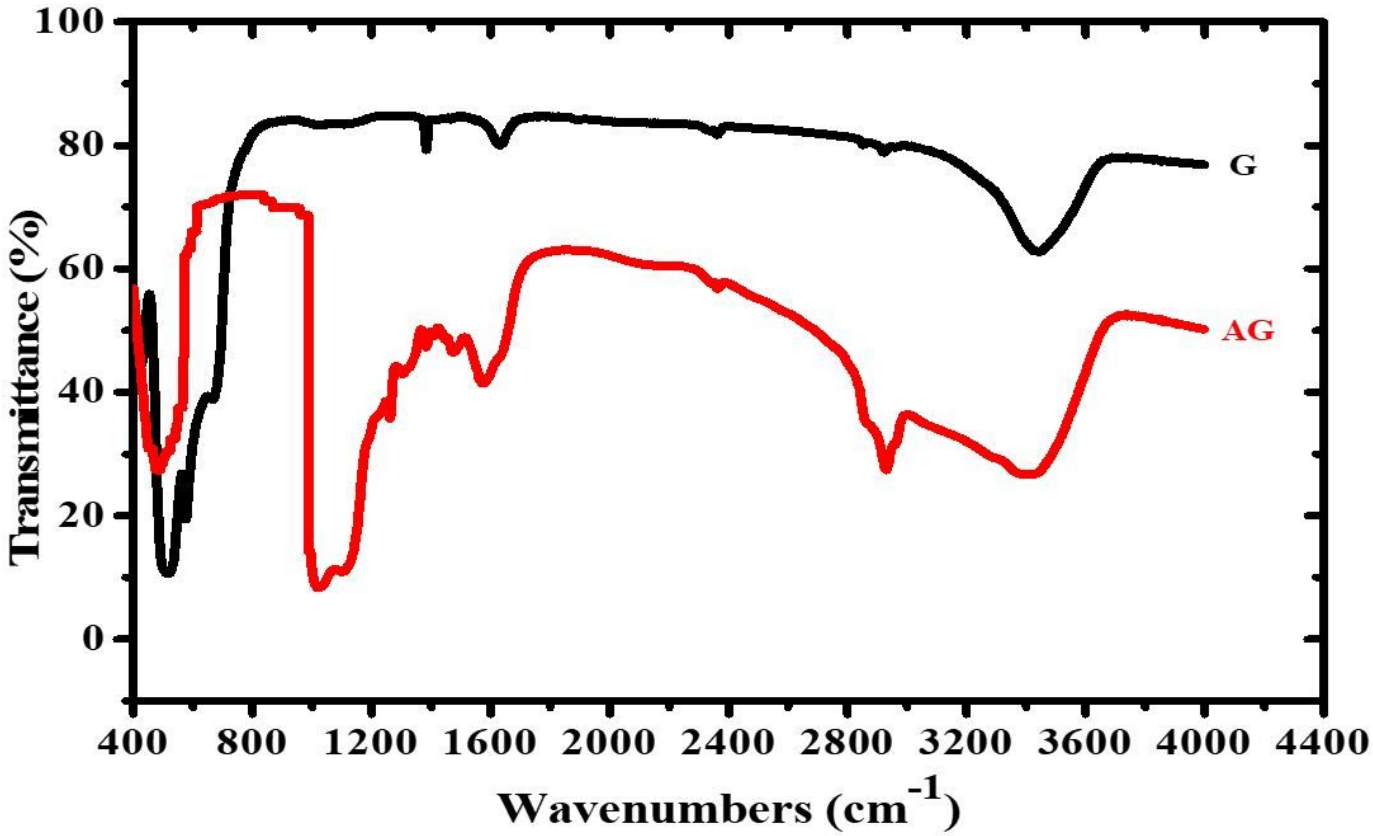

Figure 3

IR spectra of gallium oxide (G) and activated gallium oxide (AG).

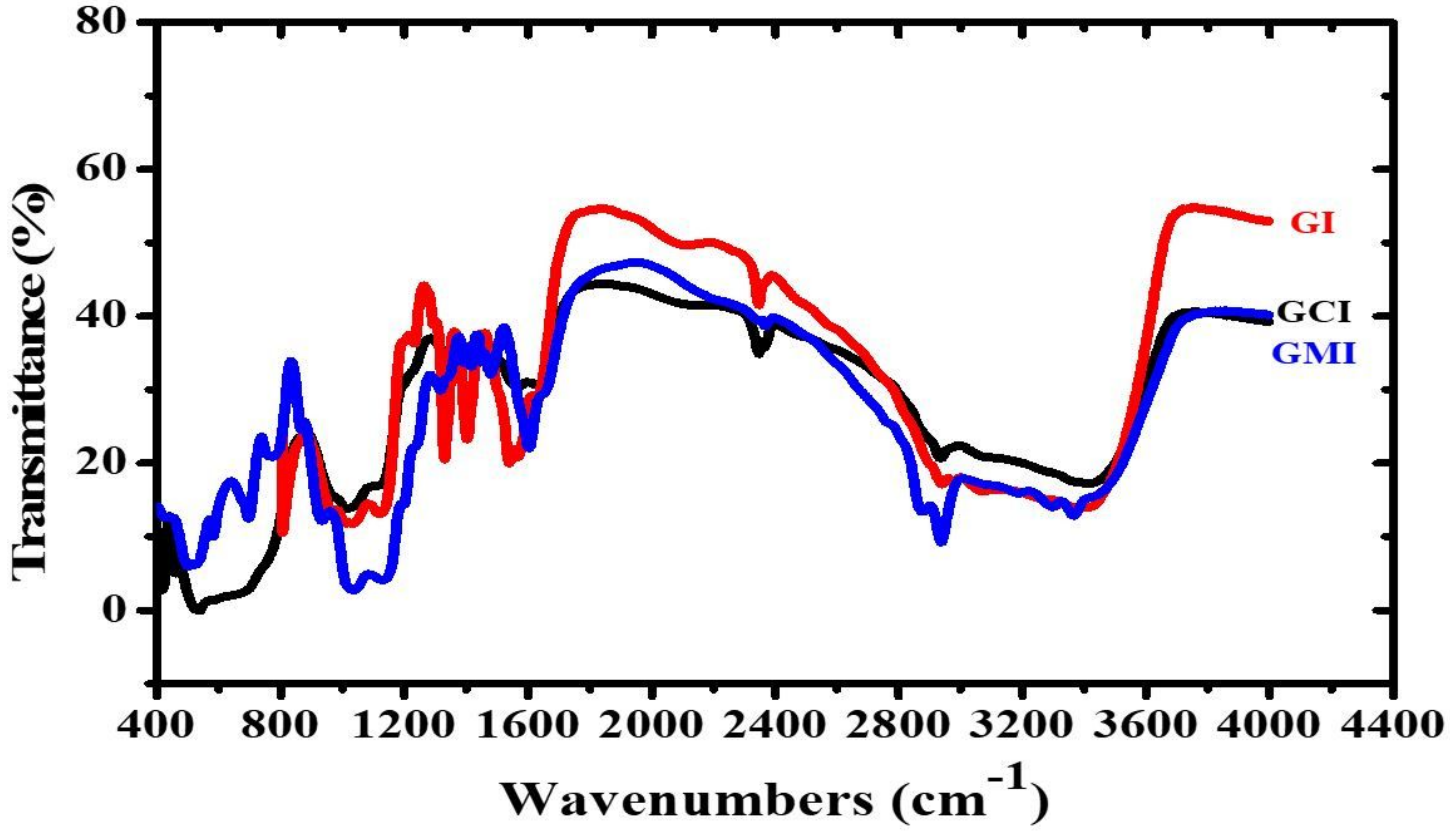

Figure 4

IR spectra of gallium hybrids, GI (a), GCI (b), and GMI (c).

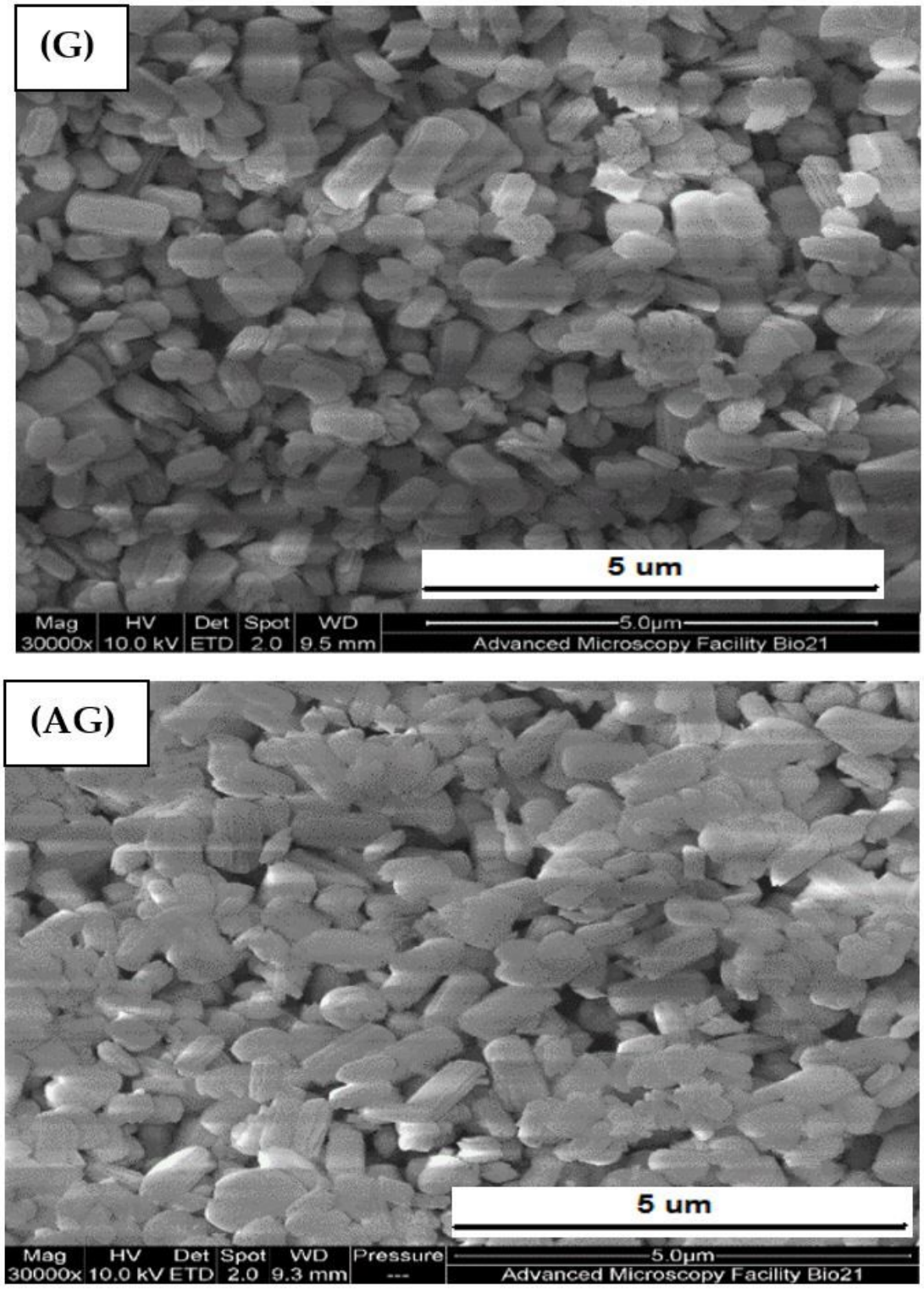

Figure 5

SEM images of gallium oxide (G) and activated gallium oxide (AG).

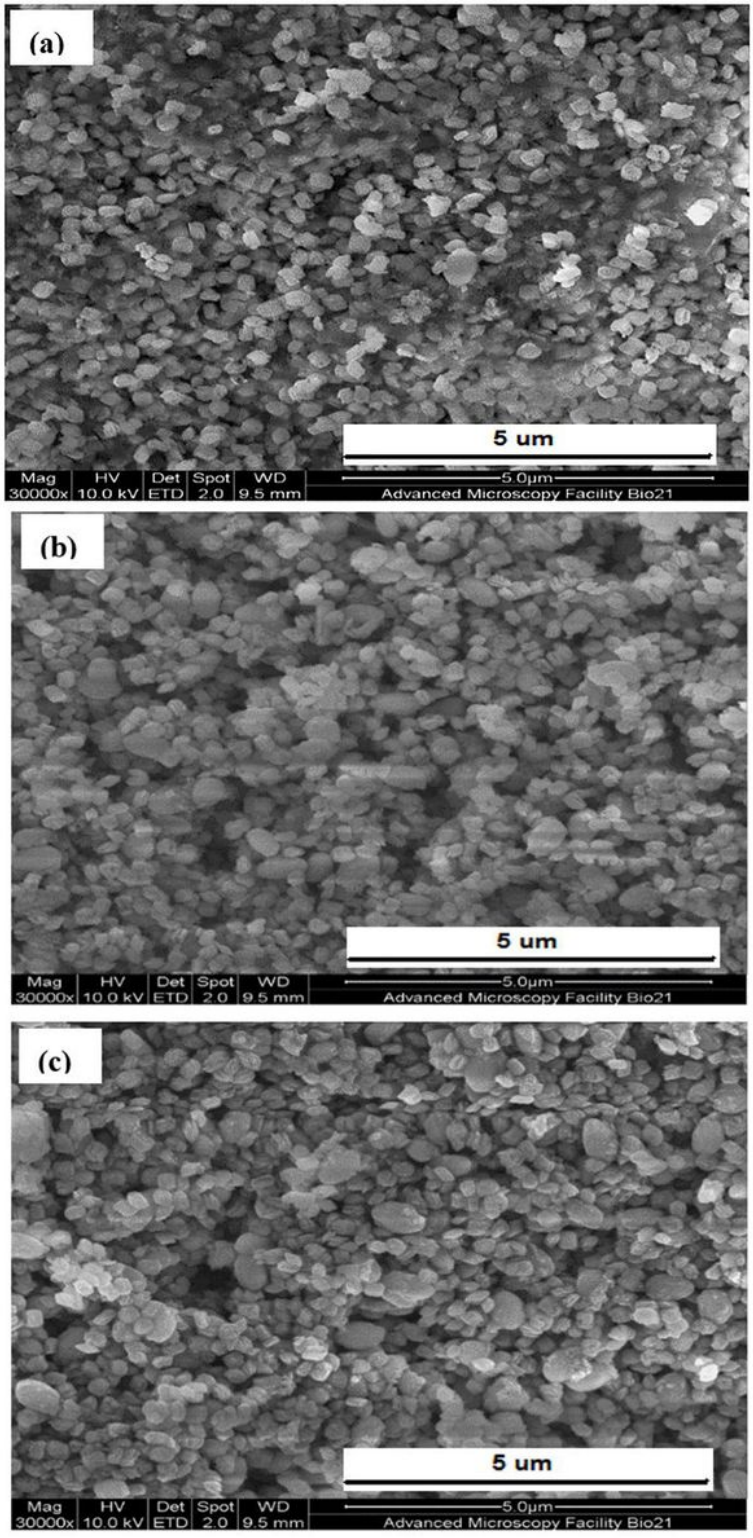

Figure 6

SEM images of gallium hybrid, GI (a), GCI (b), and GMI (c).

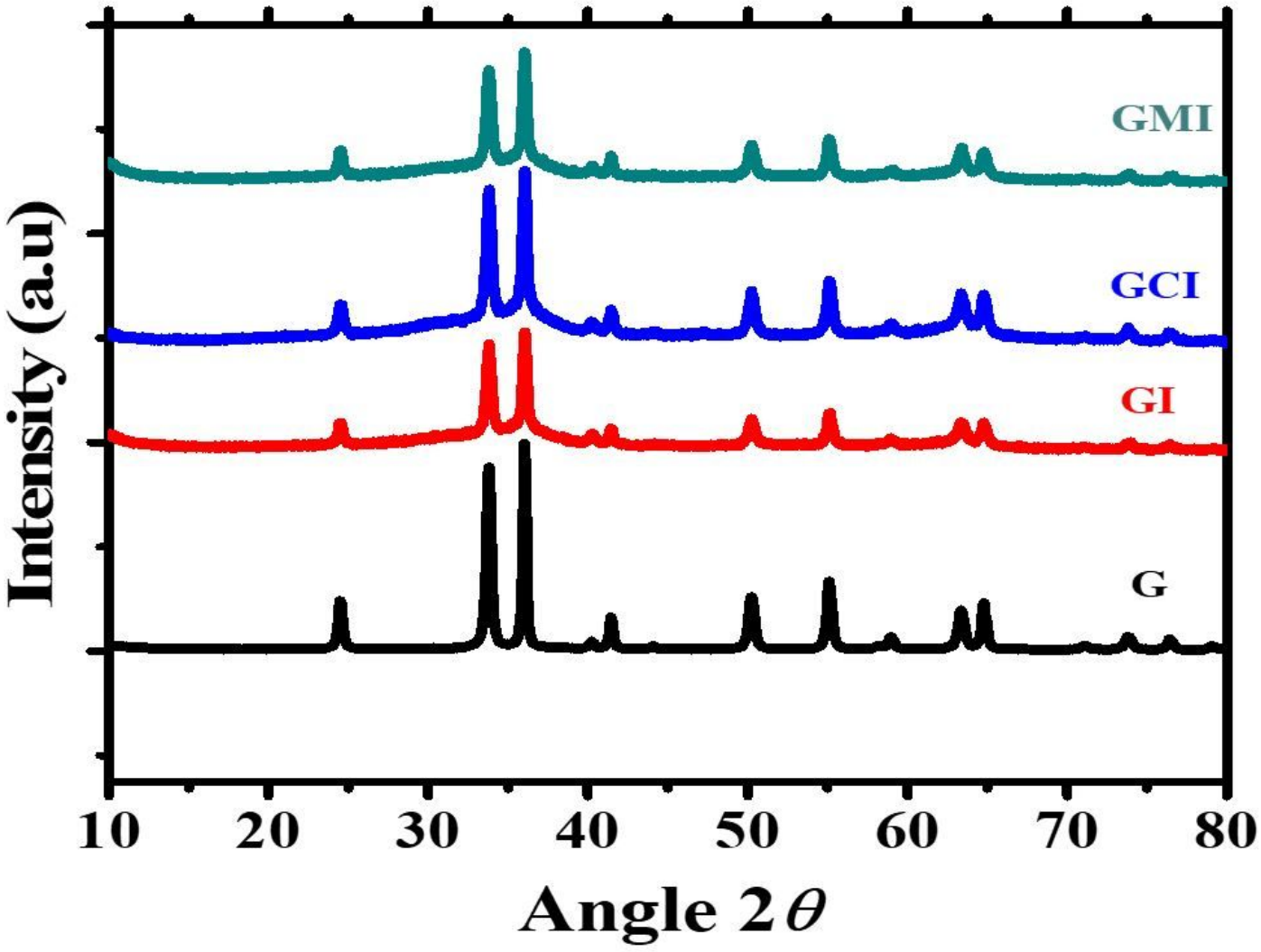

Figure 7

XRD pattern of gallium oxide (G) and gallium hybrid, GI, GCI, and GMI.

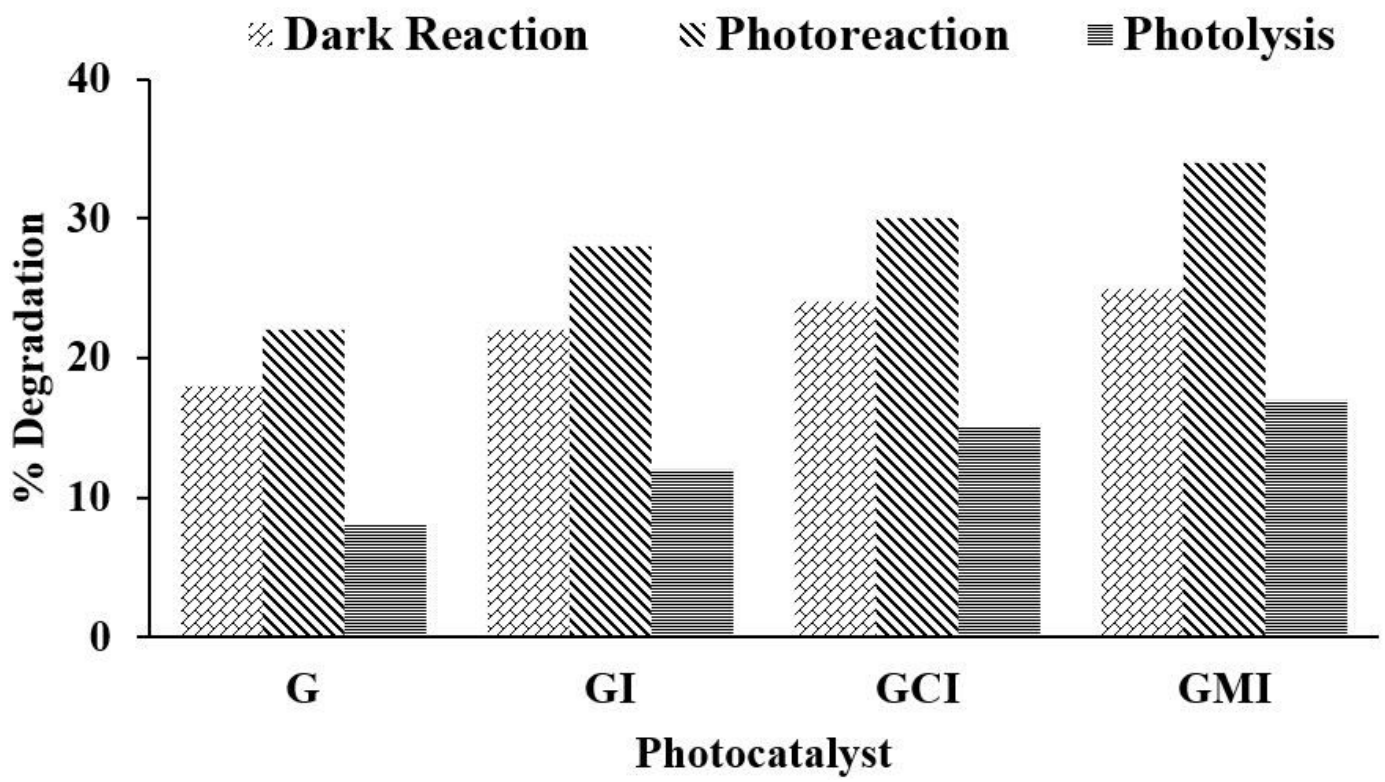

Figure 8

Dark reaction, Photolysis, and Photoreaction of Rhodamine B.

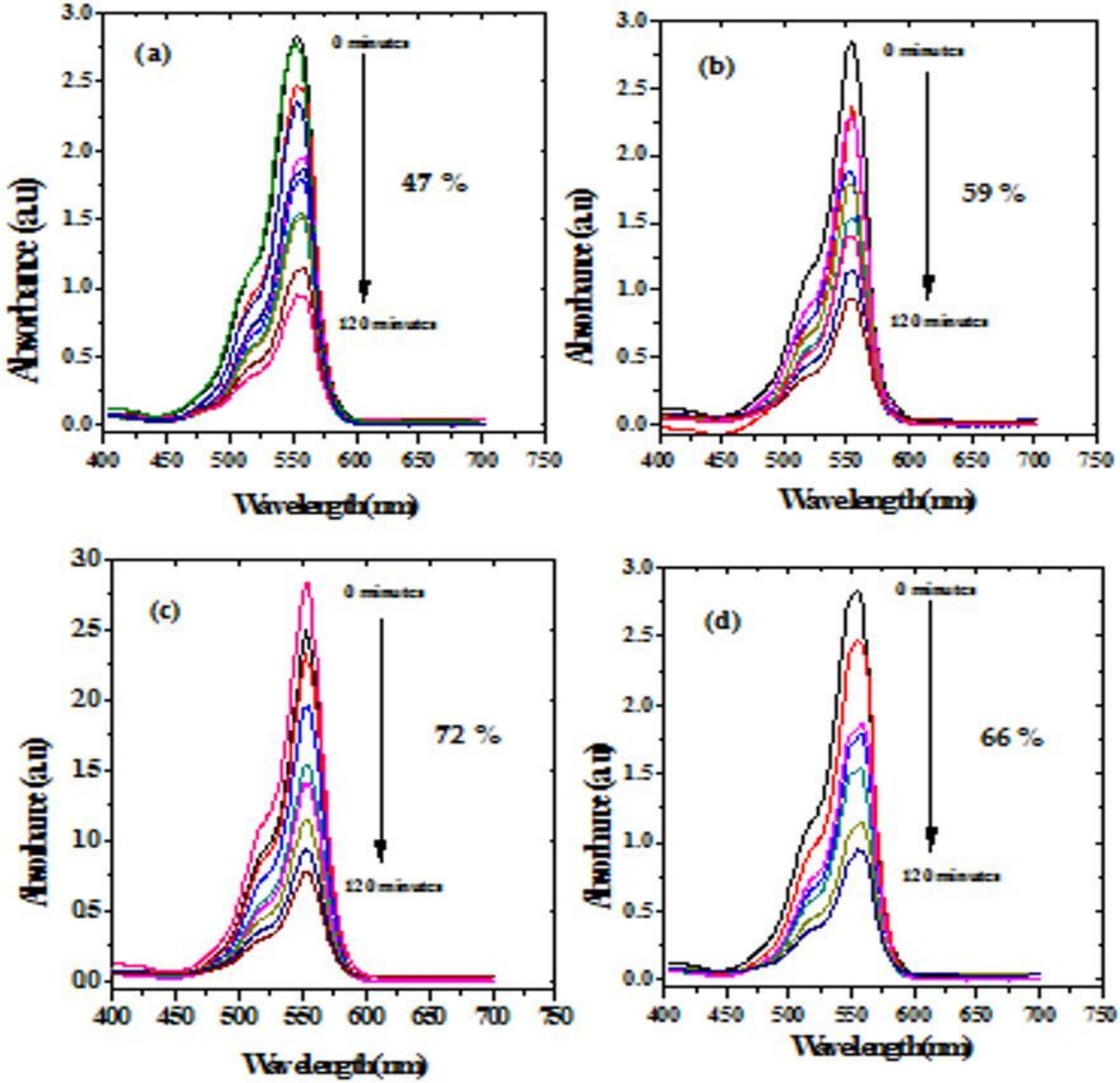

Figure 9

influence of time on the Photodegradation of Rhodamine B using gallium oxide (a) and gallium-indole (b), gallium-carboxylic indole, and gallium-methyl indole at pH 7 and 0.03mg/L

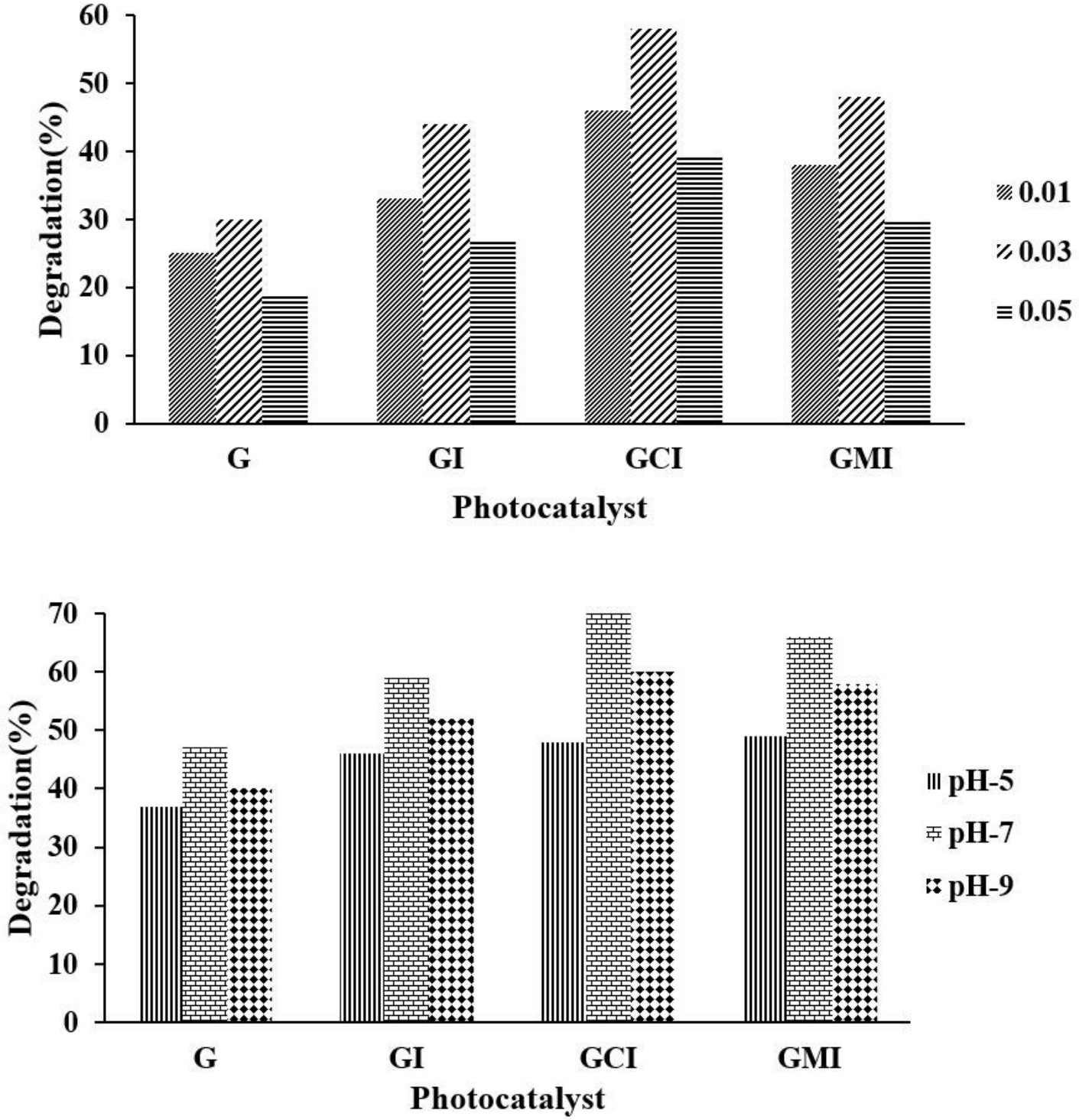

Figure 10

Influence of dye concentration (a) and pH (b) on the photodegradation of Rhodamine B.

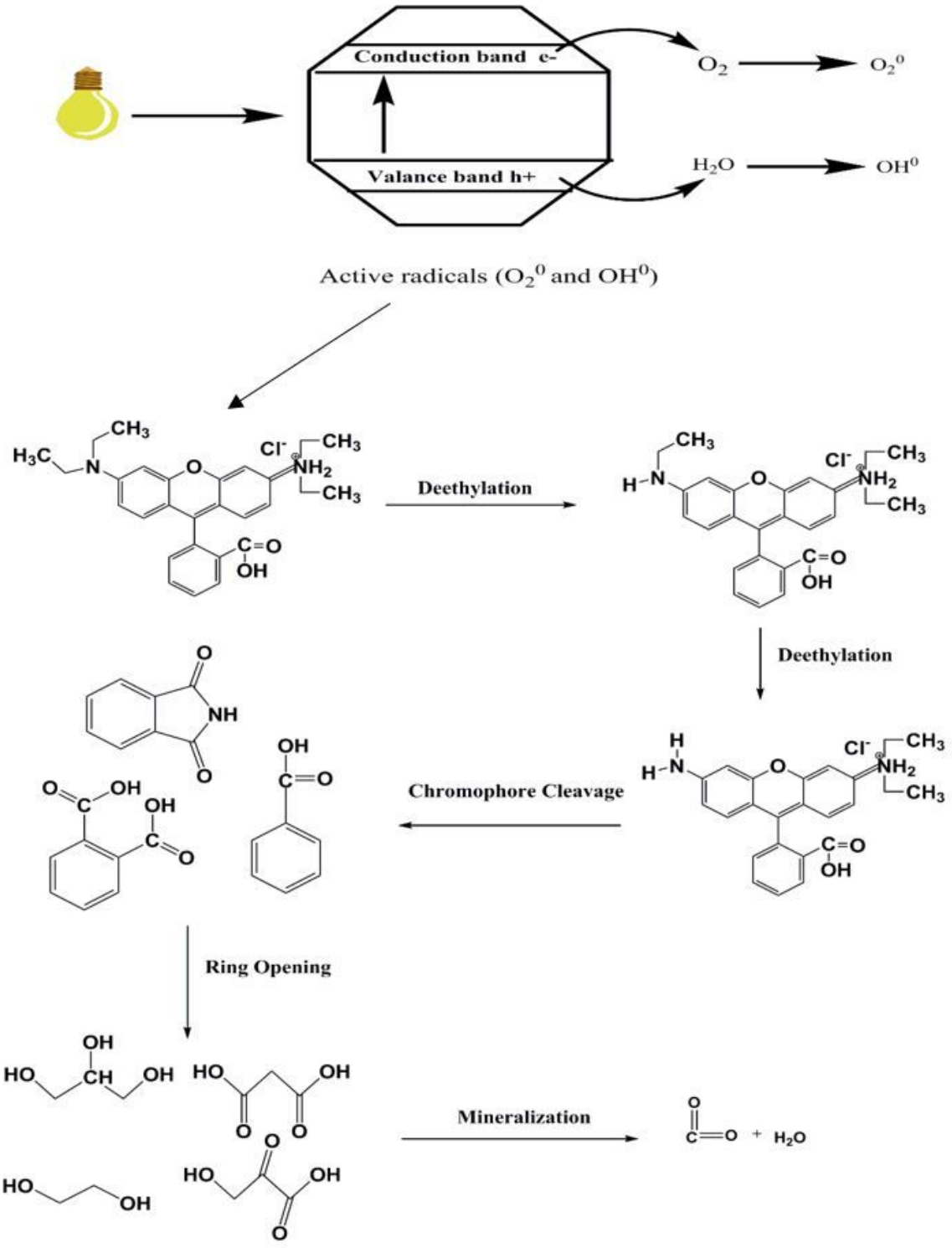

Figure 11

Proposed mechanism of Rhodamine B photo-degradation.

Supplementary Files

This is a list of supplementary files associated with this preprint. Click to download.

- Supplementaryinformationfile.docx